Received: 31 March 2023 | Revised: 29 May 2023 | Accepted: 16 June 2023

DOI: 10.1002/jbio.202300106

LETTER

JOURNAL OF BIOPHOTONICS

High-speed submillimeter magnetic-driven rotational scanning side-imaging OCT probe

Chi Zhang[1] | **Fan Yang**[1] | **Fu Wang**[1] | **Qingyue Tan**[1] | **Hao He**[1] | **Su Zhang**[1] | **Jigang Wu**[2] | **Shengxian Tu**[1]

[1]School of Biomedical Engineering, Biomedical Instrument Institute, Shanghai Jiao Tong University, Shanghai, China

[2]Biophotonics Laboratory, University of Michigan – Shanghai Jiao Tong University Joint Institute, Shanghai Jiao Tong University, Shanghai, China

Correspondence

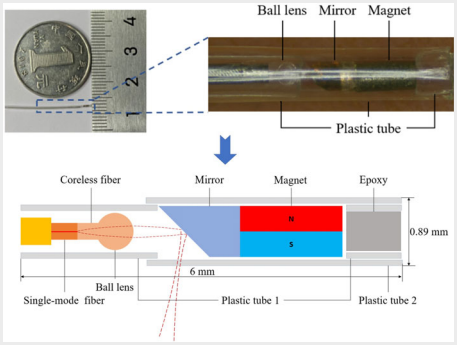
Jigang Wu, Biophotonics Laboratory, University of Michigan – Shanghai Jiao Tong University Joint Institute, Shanghai Jiao Tong University, Shanghai 200240, China.
Email: jigang.wu@sjtu.edu.cn

Shengxian Tu, School of Biomedical Engineering, Biomedical Instrument Institute, Shanghai Jiao Tong University, Shanghai 200030, China.
Email: sxtu@sjtu.edu.cn

Funding information

National Natural Science Foundation of China, Grant/Award Number: 82020108015

Abstract



A high-speed side-imaging magnetic-driven scanning (MDS) probe is proposed for endoscopic optical coherence tomography (OCT). In the distal end of the probe, a reflecting micromirror is attached to a tiny magnet, which is driven by an external fast-rotating magnetic field to achieve unobstructed 360-degree side-view scanning. A prototype probe was fabricated with an outer diameter of 0.89 mm. Using the prototype probe, OCT images of an ex vivo porcine artery with implanted stent were acquired in 100 frames per second. The OCT engine was a swept-source system, and the system sensitivity with the prototype probe was 95 dB with an output power of 6 mW. The axial and lateral resolutions of the system were 10.3 and 39.7 μm, respectively. The high-speed submillimeter MDS-OCT probe provides a promising alternative endoscopic OCT solution for intravascular imaging applications.

KEYWORDS

fiber optic probe, magnetic-driven, optical coherence tomography

1 | INTRODUCTION

Intravascular optical coherence tomography (IV-OCT) [1, 2] is widely used to identify vulnerable plaques and evaluate the efficacy of stents implantation. Generally, the OCT endoscopic probes can be divided into side-imaging probes [3–10] and forward-imaging probes [11–13] based on the direction of the imaging beam with respect to the longitudinal axis of the probe. Among them, the side-imaging probes are mostly used in intravascular imaging. Driven by the beam-scanning device, the side-imaging probe rotates at high speed to realize circumferential imaging. Based on the position of the beam-scanning device, the side-imaging probe can be divided into two types [14]: proximal scanning and distal scanning.

Most commercially available side-imaging endoscopic probes are proximal scanning, where the torque required for the rotation of the distal lens is transmitted by a long torque coil. An important component at the proximal end of the probe is fiber optic rotary joint that couples light from a fixed source fiber to the rotating probe [15–21]. Although proximal-scanning probes are generally more economical to fabricate and more compact [14],

Chi Zhang and Fan Yang authors equally contributed to this work.

 © 2023 Wiley-VCH GmbH.

they often suffer from OCT image distortion due to the need to rotate the entire probe during imaging, which can cause changes in the refractive index in the fiber as well as nonuniform rotation of the probe, especially in a significant tortuous vessel [22]. These issues could be resolved by the distal scanning schemes. In the distal scanning probe, a micromotor was placed at the distal end with a microreflector mounted on its shaft. Then the imaging light can be deflected and the vessel can be scanned circumferentially with the rotation of the micromotor shaft. Obviously, higher imaging speed could be achieved without rotating the entire probe. Nevertheless, micromotor-based distal scanning probes are high-cost and high-speed alternating current (AC) micromotors could be easily affected by external magnetic fields. In addition, the design of distal scanning parts is more challenging when taking the catheter diameter into consideration, which is usually smaller than 1 mm [14]. Furthermore, the wires used to drive the motors will block the light at certain angles and introduce artifacts in OCT images [11]. Therefore, to realize effective OCT imaging in a tortuous vessel with submillimeter probes, these issues need to be resolved.

In a study by Pang and Wu [23], a magnetic-driven scanning (MDS) probe was designed and implemented for OCT. A tiny externally driven magnet was assembled at the distal end of the probe to achieve unobstructed 360-degree circumferential scanning. The probe was verified in ex vivo pigeon's tissue and the biological structure was clearly imaged. However, the rotational scanning speed was relatively slow, with only two revolutions per minute (rpm). In addition, the outer diameter of the probe was 1.4 mm, which is significantly larger than common submillimeter proximal scanning probes. Furthermore, the probe structure is relatively complicated, so it is not conducive to manufacturing.

In this article, a novel high-speed submillimeter MDS-OCT probe with significantly improved design for distal-scanning side imaging is presented. On one hand, similar to previous design, the probe utilizes a tiny cylindrical magnet that is radially magnetized and attached to a reflective micromirror. On the other hand, the novel probe design includes two noteworthy improvements. First, two sets of electromagnets are used externally with driving AC electric signals that are 90 degrees out of phase to generate a rotating magnetic field, which drives the tiny magnets inside the probe to rotate. With the electromagnets, the scanning speed has achieved 100 revolutions per second (rps), which is 3000 times faster than the previous MDS-OCT probe. Second, instead of a gradient-index lens, a ball lens is used to focus the light, which is fabricated by fusing the fiber. In addition, the rotor part of the probe is also simplified. With these design improvements, the outer diameter of the probe has been reduced to 0.89 mm. Thus, the imaging speed and outer diameter of the novel MDS-OCT probe are comparable to the current state-of-the-art IV-OCT probes.

2 | METHODS

As shown in Figure 1, the distal scanning structures can be divided into three parts. The left part is enclosed in a polyamide (PA) plastic tube that has an outer diameter (OD) of 0.60 mm and an inner diameter (ID) of 0.40 mm. The middle part and the right part are enclosed in another PA tube that has an OD of 0.89 mm and an ID of 0.74 mm. In addition, the right part has another PA tube with an OD of 0.60 mm and an ID of 0.40 mm, which is nested in the abovementioned outer PA tube and fixed by epoxy glue.

The left part includes a single-mode fiber, a coreless fiber, and a ball lens. The single-mode fiber has a diameter of 125 μm and is passed through a protective hollow metal coil to keep concentric with the outer PA tube. The coreless fiber has a diameter of 125 μm and a length of 0.3 mm, which is used to expand the optical beam output from the single-mode fiber. The ball lens is fabricated by fusing the tip of the coreless fiber to form a ball with a diameter of 350 μm. All of the above elements have refractive indices of 1.47. The middle part is a microrotor, which consists of a reflecting mirror attaching to a tiny magnet with epoxy. The reflecting mirror is an angle-cut cylinder with a diameter of 0.5 mm and a length of 0.8 mm. The cut angle is 40 degree instead of 45 degree in order to avoid OCT signal saturation caused by specular reflection from the plastic tube. The reflection surface of the mirror is coated with gold. The radially magnetized miniature NdFeB magnet (AIC magnets, China) is a cylinder with a diameter of 0.5 mm and a length of 1.0 mm. The distance from the output of the ball lens to the center of the mirror is 0.8 mm. The PA tube in the right part is filled with epoxy, which prevents the rotor from moving axially. Overall, the rigid part of the distal end has a total length of 6 mm.

Figure 2 shows the schematic diagram of our OCT system and the electromagnets device for driving the tiny magnet inside the probe. A swept-source OCT system is used, where the swept frequency light source (THORLABS, SL132121-MEMS-VCSEL) has a center wavelength of 1300 nm and a sweep rate of 200 kHz.

To achieve circumferential scanning, an external rotating magnetic field is used to drive the tiny magnet rotor inside the probe. The rotor is the aforementioned mirrored permanent magnet with radial N and S poles.

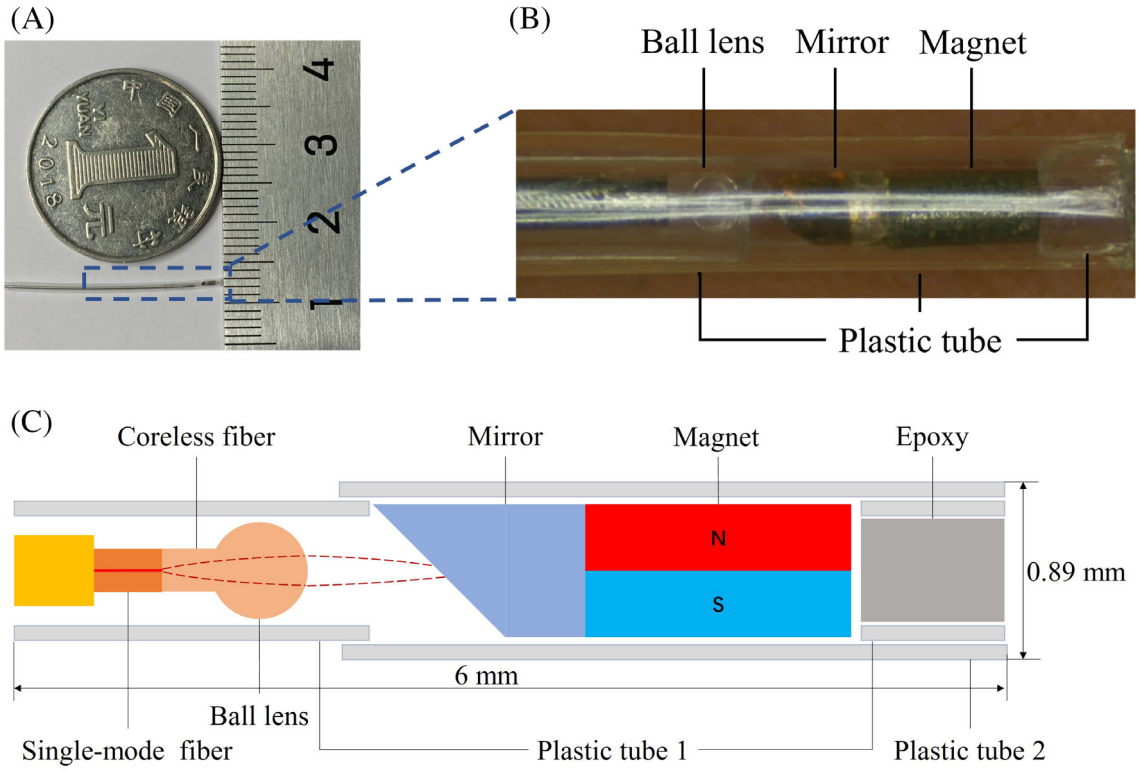


FIGURE 1 (A) A photograph of our prototype magnetic-driven scanning-optical coherence tomography probe comparing to a ruler and a coin. The outer diameter of the probe is 0.89 mm; (B) Enlarged image of probe tip; (C) The schematic of the distal end of the probe.

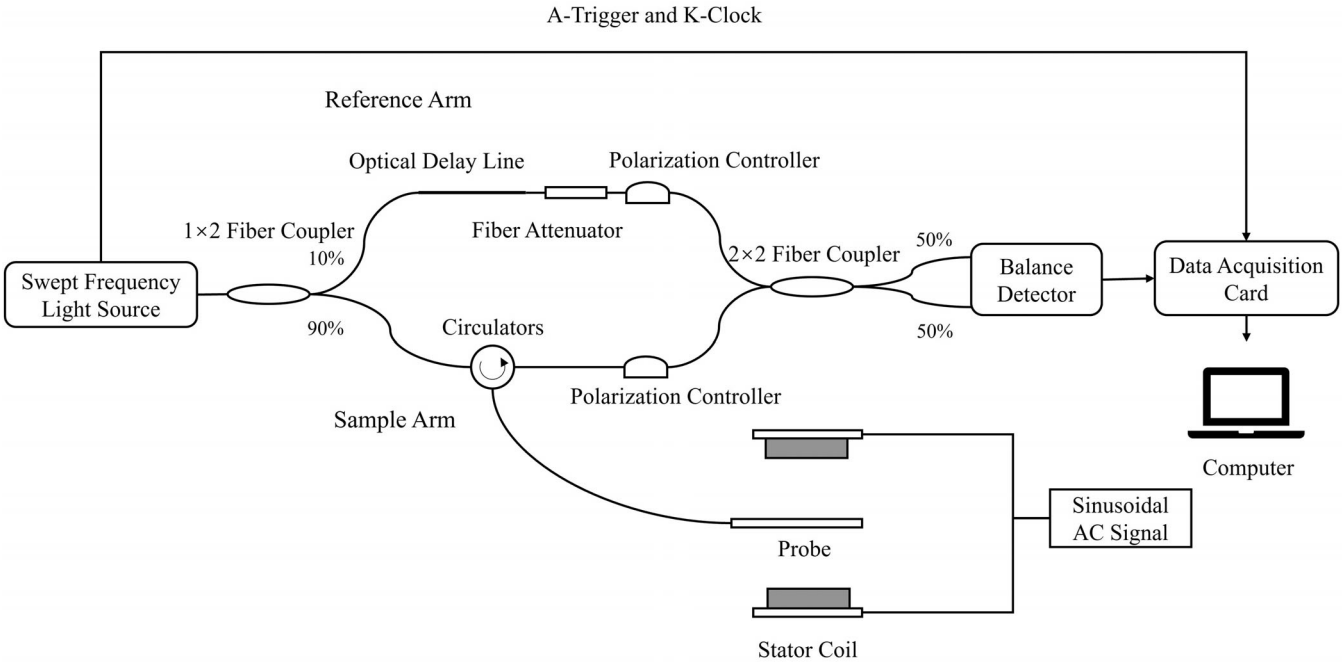


FIGURE 2 The schematic of the optical coherence tomography system integrated with the probe. AC, alternating current.

When placed in the stator magnetic field, the magnetic pole N of the stator magnetic field attracts the rotor magnetic pole S, and the stator magnetic pole S attracts the rotor magnetic pole N. Thus, when the stator poles rotate, the rotor will rotate synchronously with the stator magnetic field because of the magnetic force. In our design,

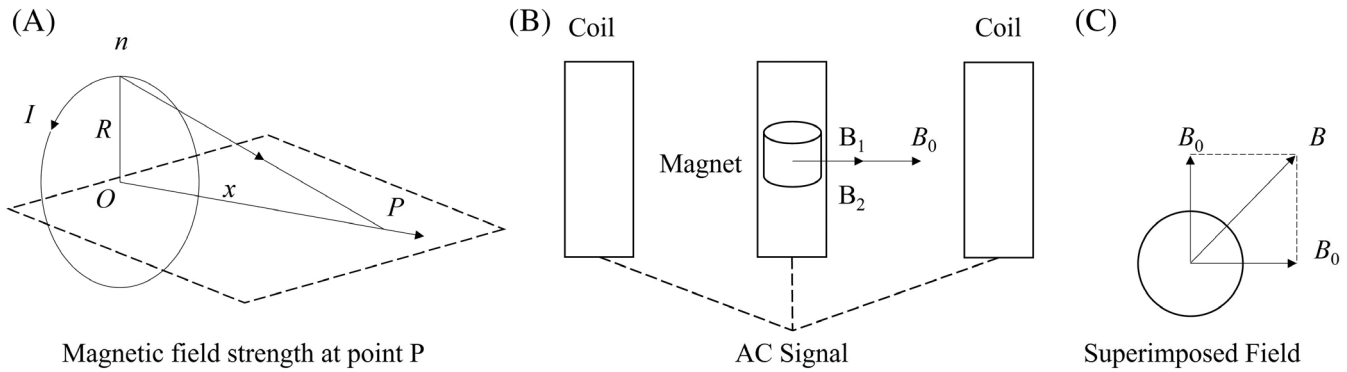


FIGURE 3 (A) Magnetic induction on the axis of n-turn energized circular coil in vacuum; (B) The schematic of the interaction between the external coil and the magnet; (C) The schematic of the superposed field applying to the magnet. AC, alternating current.

electromagnets function as the stator, where the rotating magnetic field is formed by applying an AC signal, and the stator itself does not need to rotate mechanically. The electromagnets device includes two sets of 500-turn coil windings, which are driven by two sets of sinusoidal AC currents that are of the same amplitude and 90-degree out of phase. Because of the 90-degree phase difference and the constant square sum, a stable rotating superimposed magnetic field can be generated, and the magnetic field strength is constant [24]. In the imaging experiments, the prototype probe was placed at the center of the stator and inserted into the sample. When the two sets of coils are connected to an external AC signal, the rotor inside the probe will rotate synchronously and maintain the same frequency as the external AC signal.

Compared with other types of OCT probes, there are four main advantages of our MDS-OCT probe: (1) The probe structure is simple, and the rotor consists of only a small magnet and a mirror. All the components are low cost and can be made with submillimeter size; (2) The working distance can be controlled by adjusting the distance between the ball lens and the mirror, thus the transverse resolution can be optimized for specific depth of interest; (3) Because the rotor has no electric wires, the outgoing OCT light from the probe is unobstructed during the 360-degree circumferential scanning, there is no wire artifact which commonly occurs in micromotor-based OCT probes; (4) The rotation frequency of the magnetically-controlled rotor is synchronous with the external AC signal and could achieve high rotational speed, which is suitable for OCT imaging with high frame rate.

The required distance between the external electromagnets and the probe tip, which is determined by the magnetic force, needs to be confirmed. In the following, the magnetic torque exerted on the rotor inside the probe by the two sets of coils will be estimated. Figure 3 shows a schematic diagram of the magnetic induction intensity applied by a set of coils to the probe. It is assumed that the magnetically controlled rotor is located exactly on the axis of the coil. In the following, μ_0 is the magnetic permeability in vacuum, I is the current in the coil, R is the radius of the coil, n is the number of turns of the coil, and x is the distance from the magnet to the center of the coil. According to the arrangement of the magnetic poles, B_1 and B_2 are the magnetic inductions applied to the rotor magnet by the two coils in the same direction, and B_0 is the superimposed magnetic induction of a group of coils in one direction. The directions of B_1 and B_2 are as shown in Figure 3, so the total magnetic induction B_0 applied to the rotor magnet is [25, 26].

$$B_0 = \frac{\mu_0 I R^2 n}{2(R^2+x^2)^{3/2}} \times 2 = \frac{\mu_0 I R^2 n}{(R^2+x^2)^{3/2}} \tag{1}$$

Then the mutually perpendicular superimposed magnetic induction B generated by the two sets of coils is

$$B = \sqrt{2} B_0 = \frac{\sqrt{2}\mu_0 I R^2 n}{(R^2+x^2)^{3/2}} \tag{2}$$

where the two sets of coils are assumed to be independent. The torque N applied to the rotor magnet can be written as

$$N = m \times B \tag{3}$$

where m is the total magnetic moment of the magnet that can be calculated as $m = V_r \times M$, where V_r is the volume of the rotor magnet and M is the magnetization.

For a rough estimate of the maximum allowable x, a torque of 1 μN·m is assumed to be sufficient to drive a rotor with a diameter of 0.9 mm, based on typical

figures for a micromotor of similar size [27, 28]. Since the rotor is loaded with the reflection mirror with roughly the same weight as the magnet, the required N doubles, which is 2 μN·m. Using the actual parameters $\mu_0 M = 1.6\,\mathrm{T}$ (assuming saturation magnetization) [29], and $V_r = \pi \times 0.25^2 \times 1 = 0.2\,\mathrm{mm}^3$, the required magnetic induction is calculated to be $B = 0.008\,\mathrm{T}$.

In Equation (2), the coil radius is 6.5 mm, the measured electrical impedance of the coil is 8 Ω, the AC inductance is 11 mH, and the external voltage is the sinusoidal AC current with an amplitude of 10 V and a frequency of 100 Hz, the effective value of the coil current is calculated to be 0.88 A, and the number of turns of the coil n is 500. Substitute the above values into the calculation, the distance from the magnet to the center of the coil can be calculated as $x = 10.9\,\mathrm{cm}$. In the experiments, x was chosen to be around 5 cm and the rotor rotated smoothly as expected. Obviously, if the probe manufacturing process is improved to reduce the internal friction, or stronger magnetic field is provided, a larger allowable x can be expected.

Finally, the rotational stability of the MDS-OCT probe under the magnetic field was tested. Before each experiment, we will ensure that the entire catheter is roughly perpendicular to the plane of the external magnetic field and at the center of the two sets of electrodes.

TABLE 1 Rotation test results.

Set frequency (Hz)	40	50	100
Recording a given amount of time (s)	0.38 ± 0.01	0.53 ± 0.01	0.50 ± 0.01
Number of counting rotations	15	26	49
Measured rotation speed	39.5 ± 1.0	49.1 ± 1.0	98.0 ± 2.0

This ensures that the magnetic flux vector in both directions is maximized for the small magnet, thereby maintaining rotational stability. The frequency of the external sine wave was set as 40, 50, and 100 Hz, respectively. The probe was externally connected to visible light with 650 nm wavelength for observation. The rotation of the probe was recorded by a camera with an acquisition speed of 960 frames per second. In the recorded video, it was observed that the rotation was smooth. The number of rotations was then counted within a certain period of time, and the measured rotation speed of the probe (number of rotations/recording time) was calculated. As given in Table 1, the rotation of the MDS-OCT probe is relatively stable, which can well meet the design requirements. It should be noted that in the imaging experiments, the magnetic field amplitude will be almost the same in the biological tissue as in air for static or low-frequency magnetic field [30, 31] (Figure 4).

3 | RESULTS AND DISCUSSION

Before the imaging experiments, the performance of the OCT system with our prototype probe was tested. The measured working distance from the outer surface of the probe was ~0.5 mm. The output power of the OCT system before coupling into the probe was 16 mW, and the output power of the probe was 6 mW, indicating that the probe insertion loss is 4.3 dB. We evaluated the source of loss in the probe and believe that it is mainly caused by the reflection at interface of the ball lens as well as the loss when passing through the plastic tube. The misalignment of the reflecting mirror with respect to the ball lens may also introduce additional loss. The system sensitivity with the probe was measured to be 95 dB,

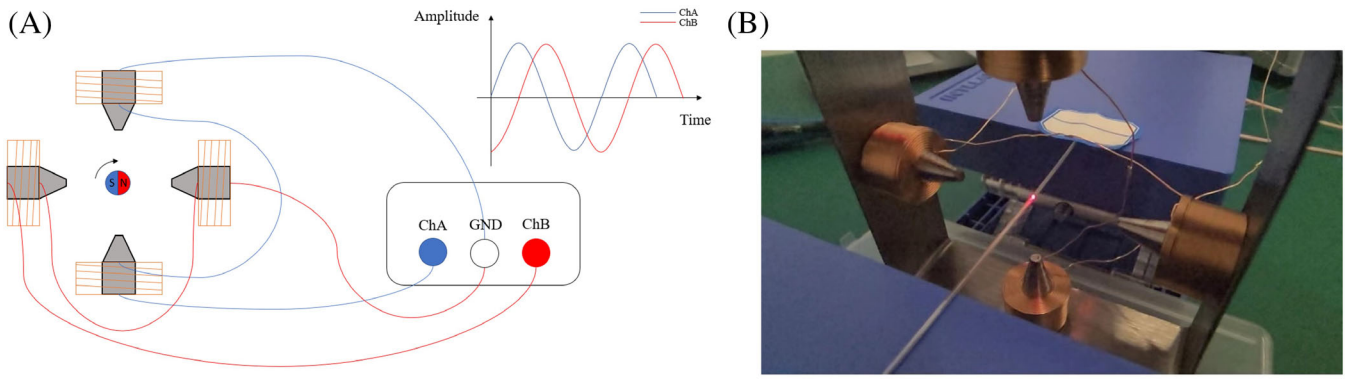


FIGURE 4 (A) The schematic diagram of the stator consisting of two pairs of electromagnets. The gray structure is a silicon steel core used to concentrate the magnetic flux (ChA, channel A; ChB, channel B); (B) A photograph of the stator and the prototype probe. A red laser with 650 nm wavelength was coupled into the probe for indicating the scanning motion.

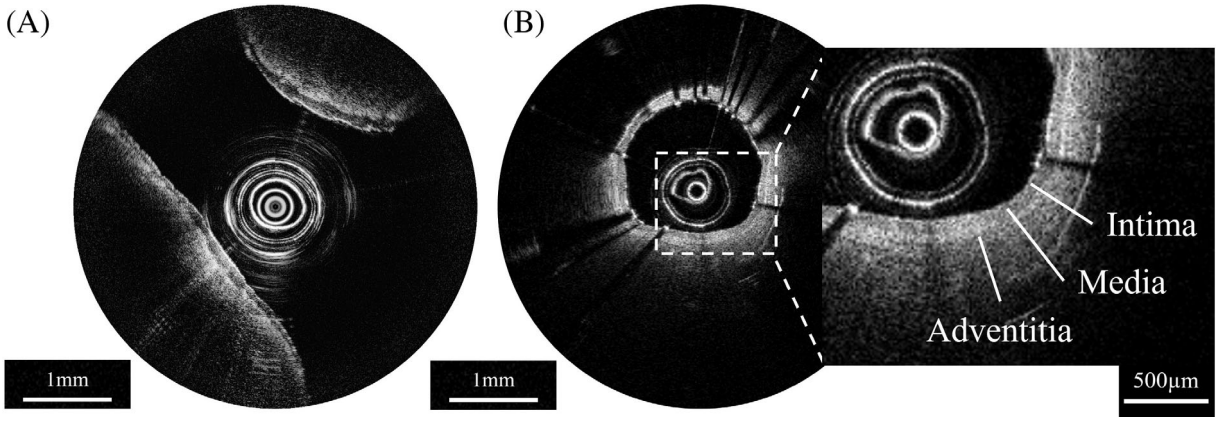


FIGURE 5 (A) Optical coherence tomography (OCT) image of a human finger. The epidermis and dermis of the skin can be distinguished clearly and accurately. (B) OCT image of an ex vivo porcine artery with implanted stent. The adventitia, media and intima of the blood vessel can be clearly identified (the deformed circle in the center of the figure is the imaging of the mirror, which is caused by the micron-scale vibration of the small magnet under the action of the magnetic field).

which could be improved by reducing the insertion loss of the probe with better fabrication technique. The axial resolution was measured as 10.3 μm and the lateral resolution was 39.7 μm, which was calculated by paraxial Gaussian beam propagation and measured by beam profiler (the calculated result of the beam spot size is about 38.0 μm and the measurement is consistent with our calculation).

First, the probe system was used to image a human finger. Then the probe system was used to scan an ex vivo porcine artery sample with an implanted stent (the vascular tissue was wrapped around the probe, and the magnetic field does not attenuate significantly in biological tissues). In the experiment, B-scan OCT images were acquired by using 2000 A-scans at a rotational scanning speed of 100 rps to form the circumferential cross-sectional image. As shown in Figure 5A, the epidermis and dermis of the skin were been distinguished clearly and accurately. As shown in Figure 5B, the stent can be clearly observed, and the adventitia, media, and intima of the artery can be discerned in the enlarged inset.

The main contributions of this study include: (1) a high-speed submillimeter MDS-OCT lateral imaging probe was designed and fabricated to overcome nonuniform rotation artifacts in tortuous blood vessels. (2) The prototype probe has achieved unobstructed high-speed 360-degree circumferential scanning without introducing obvious wire artifacts. (3) The obtained high-resolution OCT images can clearly show the biological structure of the porcine artery samples.

We note that several important factors need to be considered before applying the MDS-OCT probe into in vivo imaging, including the distance between the outer stator and the probe, the uniformity of rotational scanning, and the axial movement of the rotor.

For imaging small animals such as pigeons, mice, and rats, it is relatively easy to use the prototype setup because a small distance can be maintained between the external stator and the inner rotor to ensure sufficient magnetic torque. For larger animals and humans, however, larger space will be necessary to accommodate the sample, thus stronger magnetic fields will be required, and the use of superconducting coils may be considered. Further studies will be needed when considering whether it is necessary to use superconducting magnets. Here we would like to emphasize that even if superconducting magnets are necessary, the production of the external magnetic field is a one-time cost, while the probe is disposable. And, the cost of our probe is low because of the simple structure.

The uniformity of rotational scanning is important to ensure that the acquired images are free of nonuniform rotational distortion (NURD) [32], which is one of the major distortions in high-speed rotational scanning OCT probes. In our MDS-OCT probe, the uniformity of rotation mainly depends on the precise centering of the magnetic rotor and the friction during rotation. When the rotor position is closer to the center position, the magnetic field applied to it is closer to the previous calculation result, so the rotation is more stable. Instead, when the rotor position deviates from the center, the magnitudes of the forces exerted by the two sets of electromagnet coils are different, resulting in unstable superimposed magnetic force, thus affecting the stability of the rotation. To improve the successful rate of probe fabrication, special optical alignment devices may be considered to ensure accurate centering of the rotor. In addition, here

we would like to comparing the source of NURD in our probe and the normal commercially available probe. The main source of the traditional NURD with the rotation of the whole catheter is that the bending of catheter causes inconsistent friction during rotation, and this friction happens in the whole catheter and thus uncontrollable because the bending states varies in different situation. In contrast, the main source of NURD in our probe is the friction between the rotor and the protection tube, which is repeatable. We expect that the impact of NURD could be alleviated by adding lubricants to reduce friction, or using miniature bearings (if possible), and ensure the entire catheter manufactured in a dust-free environment to minimize friction. Thus in principle, compared with traditional probe, it should be easier to resolve the NURD issue in our probe.

The axial movement of the rotor usually appears when the rotor axis is tilted with respect to the magnetic field, which will cause the shifting of OCT A-lines during the rotational scanning, thus result in distortion of the image. In the prototype probe, this issue was resolved by limiting the space for the axial motion of the rotor by placing the PA plastic tubes precisely.

Another challenge is that when imaging in highly tortuous vessels, alignment of the small magnet with respect to the external magnetic field is important for probe rotation. As reported previously [33], a multidirectional rotating magnetic field could be designed to adjust the specific position of the probe tip three-dimensionally in a magnetic navigation surgical robot. We expect that a similar design could be applied in our probe system when necessary.

4 | CONCLUSIONS

A high-speed submillimeter MDS OCT probe was designed and implemented. The prototype probe had an outer diameter of 0.89 mm and could perform OCT imaging with 100 frames per second. The feasibility of intravascular OCT imaging using the prototype probe was demonstrated with an ex vivo porcine artery. The novel probe is promising and cost-efficient for intravascular imaging applications, and especially suitable for narrow and tortuous vessels.

FUNDING INFORMATION

National Natural Science Foundation of China (Grant No. 82020108015).

CONFLICT OF INTEREST STATEMENT

The authors declare no financial or commercial conflict of interest.

DATA AVAILABILITY STATEMENT

The data that support the findings of this study are available from the corresponding author upon reasonable request.

ORCID

Fan Yang https://orcid.org/0009-0002-9172-3142

REFERENCES

[1] D. Huang, E. A. Swanson, C. P. Lin, J. S. Schuman, W. G. Stinson, W. Chang, M. R. Hee, T. Flotte, K. Gregory, C. A. Puliafito, *Science* **1991**, *254*, 1178.

[2] W. Drexler, M. Liu, A. Kumar, T. Kamali, A. Unterhuber, R. A. Leitgeb, *J Biomed Opt* **2014**, *19*, 071412.

[3] D. Wang, L. Fu, X. Wang, Z. Gong, S. Samuelson, C. Duan, H. Jia, J. S. Ma, H. Xie, *J Biomed Opt* **2013**, *18*, 086005.

[4] G. Tearney, S. Boppart, B. Bouma, M. Brezinski, N. Weissman, J. Southern, J. Fujimoto, *Opt Lett* **1996**, *21*, 543.

[5] J. Su, J. Zhang, L. Yu, Z. Chen, *Opt Exp* **2007**, *15*, 10390.

[6] U. Sharma, J. U. Kang, *Rev Sci Instrum* **2007**, *78*, 113102.

[7] D. Lorenser, X. Yang, R. Kirk, B. Quirk, R. McLaughlin, D. Sampson, *Opt Lett* **2011**, *36*, 3894.

[8] J. Li, M. de Groot, F. Helderman, J. Mo, J. M. Daniels, K. Grünberg, T. G. Sutedja, J. F. de Boer, *Opt. Express* **2012**, *20*, 24132.

[9] P. Herz, Y. Chen, A. Aguirre, K. Schneider, P. Hsiung, J. Fujimoto, K. Madden, J. Schmitt, J. Goodnow, C. Petersen, *Opt Lett* **2004**, *29*, 2261.

[10] T. Chen, N. Zhang, T. Huo, C. Wang, J.-G. Zheng, T. Zhou, P. Xue, *J Biomed Opt* **2013**, *18*, 086011.

[11] X. Liu, M. J. Cobb, Y. Chen, M. B. Kimmey, X. Li, *Opt Lett* **2004**, *29*, 1763.

[12] J. Wu, M. Conry, C. Gu, F. Wang, Z. Yaqoob, C. Yang, *Opt Lett* **2006**, *31*, 1265.

[13] K. M. Joos, J.-H. Shen, *Biomed Opt Exp* **2013**, *4*, 1342.

[14] M. J. Gora, M. J. Suter, G. J. Tearney, X. Li, *Biomed Opt Exp* **2017**, *8*, 2405.

[15] S. H. Yun, G. J. Tearney, B. J. Vakoc, M. Shishkov, W. Y. Oh, A. E. Desjardins, M. J. Suter, R. C. Chan, J. A. Evans, I.-K. Jang, *Nat Med* **2006**, *12*, 1429.

[16] T.-H. Tsai, B. Potsaid, Y. K. Tao, V. Jayaraman, J. Jiang, P. J. Heim, M. F. Kraus, C. Zhou, J. Hornegger, H. Mashimo, *Biomed Opt Exp* **2013**, *4*, 1119.

[17] M. Sivak Jr., *Gastrointest Endosc* **2000**, *51*, 474.

[18] A. M. Rollins, R. Ung-Arunyawee, A. Chak, R. C. Wong, K. Kobayashi, M. V. Sivak, J. A. Izatt, *Opt Lett* **1999**, *24*, 1358.

[19] X. Li, S. Boppart, J. Van Dam, H. Mashimo, M. Mutinga, W. Drexler, M. Klein, C. Pitris, M. Krinsky, M. E. Brezinski, *Endoscopy* **2000**, *32*, 921.

[20] L. P. Hariri, M. B. Applegate, M. Mino-Kenudson, E. J. Mark, B. D. Medoff, A. D. Luster, B. E. Bouma, G. J. Tearney, M. J. Suter, *Chest* **2013**, *143*, 64.

[21] Y. Chen, A. Aguirre, P.-L. Hsiung, S. Desai, P. Herz, M. Pedrosa, Q. Huang, M. Figueiredo, S.-W. Huang, A. Koski, *Endoscopy* **2007**, *39*, 599.

[22] G. van Soest, J. Bosch, A. van der Steen. Alignment of intravascular optical coherence tomography movies affected by non-uniform rotation distortion. In Coherence Domain

Optical Methods and Optical Coherence Tomography in Biomedicine XII. **2008**.
[23] Z. Pang, J. Wu, *Biomed Opt Exp* **2015**, *6*, 2231.
[24] F. Blaabjerg, F. Lungeanu, K. Skaug, M. Tonnes, *IEEE Ind Appl Mag* **2004**, *10*, 24.
[25] R. Hilzinger, W. Rodewald, *Magnetic materials: fundamentals, products, properties, applications*, Vacuumschmeltze GmbH & Co KG Hanau, Munich **2013**.
[26] J. D. Jackson, *Classical electrodynamics*, American Association of Physics Teachers, California **1999**.
[27] C. Yang, X. Zhao, G. Ding, C. Zhang, B. Cai, *J Micromech Microeng* **2001**, *11*, 113.
[28] S. Dong, S. P. Lim, K. H. Lee, J. Zhang, L. C. Lim, K. Uchino, *IEEE Trans Ultrason Ferroelectr Freq Control* **2003**, *50*, 361.
[29] M. Sagawa, S. Hirosawa, H. Yamamoto, S. Fujimura, Y. Matsuura, *Jpn J Appl Phys* **1987**, *26*, 785.
[30] J. F. Schenck, *Prog Biophys Mol Biol* **2005**, *87*, 185.
[31] P. A. Bottomley, E. R. Andrew, *Phys Med Biol* **1978**, *23*, 630.
[32] M. L. Dufour, C.-E. Bisaillon, G. Lamouche, S. Vergnole, M. Hewko, F. D'Amours, C. Padioleau, M. Sowa. Tools for experimental characterization of the non-uniform rotational distortion in intravascular OCT probes. In Photonic Therapeutics and Diagnostics, VII. **2011**.
[33] K. T. Nguyen, S.-J. Kim, H.-K. Min, M. C. Hoang, G. Go, B. Kang, J. Kim, E. Choi, A. Hong, J.-O. Park, *IEEE Trans Biomed Eng* **2020**, *68*, 2490.

How to cite this article: C. Zhang, F. Yang, F. Wang, Q. Tan, H. He, S. Zhang, J. Wu, S. Tu, *J. Biophotonics* **2023**, *16*(10), e202300106. https://doi.org/10.1002/jbio.202300106